

# Coupling of pion condensate, chiral condensate and Polyakov loop in an extended NJL model

Zhao Zhang<sup>b,a,1</sup>, Yu-xin Liu<sup>b,a,2</sup>

<sup>a</sup>*Department of Physics, Peking University, Beijing 100871, P. R. China*

<sup>b</sup>*CCAST(World Laboratory), P.O. Box 8730, Beijing 100080, P. R. China*

December 15, 2019

## Abstract

The Nambu Jona-Lasinio model with a Polyakov loop is extended to finite isospin chemical potential case, which is characterized by simultaneous coupling of pion condensate, chiral condensate and Polyakov loop. The pion condensate, chiral condensate and the Polyakov loop as functions of temperature and isospin chemical potential are investigated by minimizing the thermodynamic potential of the system. The resulting  $(T, \mu_I)$  phase diagram is studied with emphasis on the critical point and Polyakov loop dynamics. The tricritical point for the pion superfluidity phase transition is confirmed and the phase transition for isospin symmetry restoration in high isospin chemical potential region perfectly coincides with the crossover phase transition for Polyakov loop. These results are in agreement with the Lattice QCD data.

PACS number(s): 12.38.Aw; 11.30.RD; 12.38.Lg;

## 1 Introduction

Confinement and chiral symmetry breaking are the fundamental properties of QCD in the nonperturbative domain. In principle, the color liberation associated with deconfinement is a phenomenon distinguishable from the chiral symmetry restoration phase transition, but it is likely that the mechanism of confinement would be closely related to chiral dynamics[1]. It has been argued that the confined vacuum necessarily breaks the chiral symmetry and the energy scale of confinement is less than the energy scale of chiral symmetry breaking:  $\Lambda_{QCD}$  for

---

<sup>1</sup>E-mail: zhaozhang@pku.edu.cn

<sup>2</sup>E-mail: yxliu@pku.edu.cn

confinement and  $\sim 4\pi f_\pi$  ( $f_\pi$  is the pion decay constant) for chiral symmetry breaking[2, 3]. In contrast with the situation at zero temperature, the lattice data at finite temperature suggest that the deconfinement phase transition and chiral symmetry phase transition occur at the same temperature[4–9]. Despite the attempts to explain above behaviors, the underlying reason is still unknown.

QCD phase diagram and thermodynamics has been the subject of intense investigation in recent years. Lattice simulations is a principle tool to explore the qualitative features of strongly interacting matter and make quantitative prediction of its properties. Over the years, this formulation has given us a wealth of information about the phase diagram and thermodynamics at finite temperature and limited chemical potential [10–18]. In response to the lattice simulation, many phenomenological models in terms of effective freedom degrees have been proposed to give an interpretation of the available lattice data and to make prediction in the region of phase diagram that can't be reached on the lattice yet.

As an effective chiral field theory, classical Nambu-Jona-Lasinio model (NJL) [19–21] can illustrate the transmutation of originally light quark or massless quark into massive quansiparticles and generate the pions as GoldStone bosons of spontaneously broken chiral symmetry at the same time. This type models have also been used extensively to explore color superconductivity phase transition at high baryon density[22]. However, NJL models have a principle deficiency. The reduction of the local color symmetry to the global color symmetry leads to quarks not confined in standard NJL. To cure this problem, an improved field theoretical quasi-particle model, a synthesis of Polyakov loop dynamics with NJL(PNJL), has been proposed to interpret the Lattice QCD results and extrapolate into the regions not accessible by lattice simulations [23–28]. For the chiral symmetry breaking, chiral condensate can be used as an order parameter for chiral phase transition in the chiral limit. In contrast, the deconfinement phase transition has a definite meaning only at an infinite quark mass, which the expectation value of Polyakov loop serves as an order parameter. Since the  $Z(3)$  center symmetry is explicitly broken in the real world with finite quark mass, no rigorous order parameter is established for deconfinement phase transition[29]. However, the Polyakov loop can still act as an indicator of a rapid crossover towards deconfinement for finite quark mass. The motivation behind the PNJL model is to unify the aspects of chiral symmetry breaking and confinement through introducing both the chiral condensate and the Polyakov loop as classical, homogeneous fields which simultaneously couple to quarks according the symmetry and symmetry breaking patterns of QCD.

The effectiveness of PNJL model has been tested in the literature by confronting the PNJL results with the Lattice QCD data. It has been reported that the two flavor PNJL model can reproduce the result that the crossovers for deconfinement phase transition and the chiral phase transition almost coincide[25, 28]. For finite quark chemical potential, further investigations also

suggest that the thermodynamics and susceptibilities obtained in PNJL model are excellently in agreement with the corresponding Lattice QCD data[28, 30, 32]. In addition, the PNJL model has been extended to include the diquark degrees of freedom and used to explore the phase diagrams in high baryon chemical potential[33]. Though the PNJL results have a satisfactory agreement with some lattice data, there still need to perform further test of the PNJL since for finite baryon chemical potential the available lattice simulation is limited only in the low region.

It is well known that there is no sign problem for the lattice calculation for the case with finite isospin chemical potential and zero baryon chemical potential[34–37]. Therefore, it is interesting to investigate the phase diagram and thermodynamics in the framework of PNJL model at finite isospin chemical potential and compare the results with the corresponding lattice data. In [38], the authors have extended the PNJL to the case with low baryon and isospin chemical potential without considering the pion condensate. Both the QCD effective field theory[34] and lattice calculations[35–37] have shown that the pion superfluidity phase (charged pion Boson-Einstein condensate) may occur in high enough isospin chemical potential. This phase had also been explored by other chiral models of QCD such as Ladder QCD[39], NJL model[40–42], random matrix model[43] and global color model[45]. Therefore, it is necessary to extend the PNJL model to high isospin density region to investigate the influence of Polyakov loop dynamics on the phase structure by including the pion condensate degrees of freedom and give further test of the validity of the PNJL by confronting the corresponding Lattice QCD data. In addition, due to the limitation of lattice simulation, the talk between effective fields theory and Lattice QCD is needed.

The primary purposes of this paper is to derive the formulation of the PNJL model with simultaneously considering the pion condensate, chiral condensate and Polyakov loop degrees of freedom at mean field level and then use it to explore the phase diagram of two flavor QCD to compare with the corresponding lattice data. The emphases will be put on the critical point and the impact of Polyakov loop dynamics. For simplicity, the freedom degrees of diquark is not included in this paper and the baryon chemical potential is limited in low region.

## 2 PNJL model at finite isospin chemical potential

Extending the work [28] to finite baryon chemical potential and isospin chemical potential case, the lagrangian of two-flavor PNJL model is given by

$$\mathcal{L}_{PNJL} = \bar{\psi} \left( i\gamma_{\mu} D^{\mu} + \gamma_0 \hat{\mu} - \hat{n}_0 - i\hat{\lambda} \gamma_5 \tau_1 \right) \psi + G \left[ (\bar{\psi}\psi)^2 + (\bar{\psi} i\gamma_5 \vec{\tau} \psi)^2 \right] - \mathcal{U}(\Phi[A], \bar{\Phi}[A], T), \quad (1)$$

where  $\psi = (\psi_u, \psi_d)^T$  is the quark field,

$$D^{\mu} = \partial^{\mu} - iA^{\mu} \quad \text{and} \quad A^{\mu} = \delta_{\mu 0} A^0. \quad (2)$$

The two-flavor current quark mass matrix is  $\hat{m}_0 = \text{diag}(m_u, m_d)$  and we shall work in the isospin symmetric limit with  $m_u = m_d \equiv m_0$ . The quark chemical potential matrix  $\hat{\mu}$  takes the form

$$\hat{\mu} = \begin{pmatrix} \mu_u & \\ & \mu_d \end{pmatrix} = \begin{pmatrix} \mu + \mu_I & \\ & \mu - \mu_I \end{pmatrix}, \quad (3)$$

with

$$\mu = \frac{\mu_u + \mu_d}{2} = \frac{\mu_B}{3} \quad \text{and} \quad \mu_I = \frac{\mu_u - \mu_d}{2}, \quad (4)$$

where  $\mu_B$  is baryon chemical potential corresponding to conserved baryon charge and  $\mu_I$  is isospin chemical potential corresponding to conserved isospin charge. A term proportional to  $\lambda$  is introduced in (1) which explicit break the  $U_{I_3}(1)$  symmetry (Below we call it  $I_3$  symmetry). A local, chirally symmetric scalar-pseudoscalar four-point interaction of the quark fields is introduced with an effective coupling strength  $G$ .

In comparison with the classical NJL lagrangian, the gauge field term  $A^\mu(x) = g\mathcal{A}_a^\mu(x)\frac{\lambda_a}{2}$  is contained and an effective potential  $\mathcal{U}(\Phi, \bar{\Phi}, T)$  expressed in terms of the traced Polyakov loop  $\Phi = (\text{Tr}_c L)/N_c$  and its (charge) conjugate  $\bar{\Phi} = (\text{Tr}_c L^\dagger)/N_c$  in the PNJL lagrangian. The Polyakov loop  $L$  is a matrix in colour space explicitly given by

$$L(\vec{x}) = \mathcal{P} \exp \left[ i \int_0^\beta d\tau A_4(\vec{x}, \tau) \right], \quad (5)$$

with  $\beta = 1/T$  the inverse temperature and  $A_4 = iA^0$ . In a convenient gauge (the so-called Polyakov gauge), the Polyakov loop matrix can be given a diagonal representation [29]. The coupling between Polyakov loop and quarks is uniquely determined by the covariant derivative  $D_\mu$  in the PNJL Lagrangian (1). For simplicity, the temporal component of Euclidean gauge field  $A_4$  is treated as a constant in PNJL, and the Polyakov loop is reduced as

$$L = \left[ \mathcal{P} \exp \left( i \int_0^\beta A_4 d\tau \right) \right] = \exp \left[ \frac{iA_4}{T} \right]. \quad (6)$$

Corresponding to above expression, the trace of the Polyakov loop,  $\Phi$ , and its conjugate,  $\bar{\Phi}$ , are treated as classical field variables in PNJL.

The temperature dependent effective potential  $\mathcal{U}(\Phi, \bar{\Phi}, T)$  is used to mimic pure-gauge Lattice QCD data, which should have exact  $Z(3)$  center symmetry. In this paper, we will use the potential  $\mathcal{U}(\Phi, \bar{\Phi}, T)$  proposed in [28], which takes the form

$$\frac{\mathcal{U}(\Phi, \bar{\Phi}, T)}{T^4} = -\frac{b_2(T)}{2} \bar{\Phi}\Phi - \frac{b_3}{6} (\Phi^3 + \bar{\Phi}^3) + \frac{b_4}{4} (\bar{\Phi}\Phi)^2 \quad (7)$$

with

$$b_2(T) = a_0 + a_1 \left( \frac{T_0}{T} \right) + a_2 \left( \frac{T_0}{T} \right)^2 + a_3 \left( \frac{T_0}{T} \right)^3. \quad (8)$$

A precision fit of the coefficients  $a_i$ ,  $b_i$  is performed to reproduce the lattice data and  $T_0 = 270\text{MeV}$  is adopted in this paper.

To describe the spontaneous chiral symmetry breaking and  $I_3$  symmetry breaking, we define the chiral condensate as

$$\langle \bar{\psi}\psi \rangle = \sigma = \sigma_u + \sigma_d, \quad (9)$$

with  $\sigma_u = \langle \bar{u}u \rangle$  and  $\sigma_d = \langle \bar{d}d \rangle$ , and the charged pion condensates

$$\langle \bar{\psi}i\gamma_5\tau_+\psi \rangle = \pi^+ = \frac{\pi}{\sqrt{2}}e^{i\theta}, \quad \langle \bar{\psi}i\gamma_5\tau_-\psi \rangle = \pi^- = \frac{\pi}{\sqrt{2}}e^{-i\theta}, \quad (10)$$

where  $\tau_{\pm} = (\tau_1 \pm \tau_2)/\sqrt{2}$  and  $\tau_i$  is the Pauli matrix in flavor space. In the chiral limit, nonzero condensate  $\sigma$  indicates spontaneous chiral symmetry breaking, and nonzero condensate  $\pi$  indicates spontaneous  $I_3$  symmetry breaking. The phase factor  $\theta$  describes the direction of the  $I_3$  symmetry breaking. For convenience, we adopt  $\theta = 0$  in the following and the pion condensate can be expressed as

$$\langle \bar{\psi}i\gamma_5\tau_1\psi \rangle = \pi. \quad (11)$$

This choice of the  $I_3$  symmetry breaking direction is consistent with the form of the explicit isospin breaking term introduced in (1).

Using the standard bosonization techniques, the mean field lagrangian of PNJL takes the form

$$\mathcal{L}_{\text{mf}} = \bar{\psi} (i\gamma_{\mu}D^{\mu} + \gamma_0\hat{\mu} - M - Ni\gamma_5\tau_1) \psi - G [\sigma^2 + \pi^2] - \mathcal{U}(\Phi[A], \bar{\Phi}[A], T), \quad (12)$$

with the gaps

$$M = m_0 - 2G\sigma, \quad (13)$$

$$N = \lambda - 2G\pi. \quad (14)$$

The thermal dynamical potential in the mean field level is expressed as

$$\begin{aligned} \Omega &= \mathcal{U}(\Phi, \bar{\Phi}, T) + G(\sigma^2 + \pi^2) - \frac{T}{V} \text{ln det } S_{\text{mf}}^{-1} \\ &= \mathcal{U}(\Phi, \bar{\Phi}, T) + G(\sigma^2 + \pi^2) - T \sum_n \int \frac{d^3p}{(2\pi)^3} \text{Tr ln } \frac{S_{\text{mf}}^{-1}(i\omega_n, \vec{p})}{T}, \end{aligned} \quad (15)$$

where the sum is taken over Matsubara frequencies  $w_n = (2n+1)\pi T$  and the trace is taken over color, flavor and Dirac indices. The momentum dependent inverse quark propagator matrix including both chiral and pion condensates in flavor space takes the form

$$S_{\text{mf}}^{-1}(i\omega_n, \vec{p}) = \begin{pmatrix} (i\omega_n + \mu + \mu_I + iA_4)\gamma_0 - \vec{\gamma} \cdot \vec{p} - M & -i\gamma_5 N \\ -i\gamma_5 N & (i\omega_n + \mu - \mu_I + iA_4)\gamma_0 - \vec{\gamma} \cdot \vec{p} - M \end{pmatrix}. \quad (16)$$

Using the identity  $\text{Tr} \ln(X) = \ln \det(X)$  and the technique

$$\det \begin{pmatrix} A & B \\ C & D \end{pmatrix} = \det(A)\det(B)\det(C)\det(C^{-1}DB^{-1} - A^{-1}), \quad (17)$$

the thermal dynamical potential(15) can be further expressed as

$$\begin{aligned} \Omega = & G(\sigma^2 + \pi^2) + \mathcal{U}(\Phi, \bar{\Phi}, T) - 2N_c \int \frac{d^3p}{(2\pi)^3} [E_p^- + E_p^+] \theta(\Lambda^2 - \vec{p}^2) \\ & - 2T \int \frac{d^3p}{(2\pi)^3} \text{Tr}_c \left[ \ln[1 + L^+ e^{-(E_p^- + \mu)/T}] + \ln[1 + L e^{-(E_p^- - \mu)/T}] \right. \\ & \left. + \ln[1 + L^+ e^{-(E_p^+ + \mu)/T}] + \ln[1 + L e^{-(E_p^+ - \mu)/T}] \right], \end{aligned} \quad (18)$$

with quasiparticle energy  $E_p^\pm = \sqrt{(E_p \pm \mu_I)^2 + N^2}$  and  $E_p = \sqrt{\vec{p}^2 + M^2}$ . Performing the remaining color trace, the integrand of last term on r.h.s. (18) is given by

$$\begin{aligned} & \ln \det \left[ 1 + L e^{-(E_p^- - \mu)/T} \right] + \ln \det \left[ 1 + L^+ e^{-(E_p^- + \mu)/T} \right] \\ & + \ln \det \left[ 1 + L e^{-(E_p^+ - \mu)/T} \right] + \ln \det \left[ 1 + L^+ e^{-(E_p^+ + \mu)/T} \right] \\ = & \ln \left[ 1 + 3 \left( \Phi + \bar{\Phi} e^{-(E_p^- - \mu)/T} \right) e^{-(E_p^- - \mu)/T} + e^{-3(E_p^- - \mu)/T} \right] \\ & + \ln \left[ 1 + 3 \left( \bar{\Phi} + \Phi e^{-(E_p^- + \mu)/T} \right) e^{-(E_p^- + \mu)/T} + e^{-3(E_p^- + \mu)/T} \right] \\ & + \ln \left[ 1 + 3 \left( \Phi + \bar{\Phi} e^{-(E_p^+ - \mu)/T} \right) e^{-(E_p^+ - \mu)/T} + e^{-3(E_p^+ - \mu)/T} \right] \\ & + \ln \left[ 1 + 3 \left( \bar{\Phi} + \Phi e^{-(E_p^+ + \mu)/T} \right) e^{-(E_p^+ + \mu)/T} + e^{-3(E_p^+ + \mu)/T} \right]. \end{aligned} \quad (19)$$

From (18) and (19), we see that the trace of the Polyakov loop  $\Phi$  and its conjugate  $\bar{\Phi}$  can still be factored out despite the appearance of the off-diagonal terms in the inverse quark propagator. It is easy seen from (19) that the classical NJL model is restored from PNJL when  $\Phi$  and  $\bar{\Phi}$  approach 1.

Minimizing the thermal dynamical potential (18), the motion equations for the mean fields  $\sigma$ ,  $\pi$ ,  $\Phi$  and  $\bar{\Phi}$  are determined through the coupled equations

$$\frac{\partial \Omega}{\partial \sigma} = 0, \quad \frac{\partial \Omega}{\partial \pi} = 0, \quad \frac{\partial \Omega}{\partial \Phi} = 0, \quad \frac{\partial \Omega}{\partial \bar{\Phi}} = 0. \quad (20)$$

This set of equations is then solved for the fields  $\sigma$ ,  $\pi$ ,  $\Phi$  and  $\bar{\Phi}$  as functions of the temperature  $T$ , baryon chemical potentials  $\mu_B$  and isospin chemical potential  $\mu_I$ . Note that when there exist multi roots of these coupled equations, the solution corresponding to the minimal thermodynamical potential is favored.

The NJL part of the model involves three parameters: the current quark mass of  $u$  and  $d$ , the local four fermion coupling constant  $G$  and the three-momentum cutoff  $\Lambda$ . In this work, these

parameter are fixed to reproduce three physical quantities in vacuum: pion mass  $m_\pi = 140\text{MeV}$ , pion decay constant  $f_\pi = 93\text{MeV}$  and chiral condensate  $\langle\bar{u}u\rangle = \langle\bar{d}d\rangle = \sigma_0/2 = -(250\text{MeV})^3$  with

$$m_0 = 5.5\text{MeV}, \quad G = 5.04\text{GeV}^{-2}, \quad \Lambda = 0.651\text{GeV}. \quad (21)$$

Once  $\Omega$  is known, the thermodynamic functions that measure the bulk properties of matter can be obtained. For an infinite system, the pressure  $p$ , the entropy density  $s$ , the baryon number density  $n_B$ , the isospin number density  $n_I$ , the flavor number density  $n_u$  and  $n_d$ , the energy density  $\epsilon$  and the specific heat  $c$  are all derived from  $\Omega$ .

For  $\mu_B = 0$ , the trace of Polyakov loop  $\Phi$  is equal to its conjugate  $\bar{\Phi}$  and both fields are real. Without concerning the isospin chemical potential, numerical results suggests that the crossover phase transitions for the chiral condensate  $\sigma$  and for the Polyakov loop  $\Phi$  almost coincide in PNJL and the difference between the two transition temperatures is within  $5\text{MeV}$ [28, 30]. Following[28], we define  $T_c$  as the average of the two transition temperature and we verified the result that  $T_c^0 = 227\text{MeV}$  [30] for  $\mu_B = \mu_I = 0$ . Since the PNJL model uses a simple static background field representing the Polyakov loop and reduce the gluon dynamics to chiral point couplings between quarks, this model can not be expected to work beyond a limited temperature and quark chemical potential. It is assumed this model works up to an upper limit of temperature with  $T \leq (2 - 3)T_c^0$  because the transverse gluon degrees of freedom will be important for  $T > 2.5T_c^0$ [31]. In this paper we only consider the case for  $\mu_B = 0$  and we assume that PNJL works well in the region  $|\mu_I| < 500\text{MeV}$

### 3 Results

#### 3.1 For $\lambda = 0$ and $\mu_B = 0$

For  $\lambda = 0$ , the charged pion condensate  $\pi$  is the true order parameter for the pion superfluidity phase transition. Previous investigations based on the QCD effective field theory[34] and lattice simulations[35–37] have shown that pion superfluidity phase occurs when  $\mu_I > \mu_c = m_\pi/2$  for  $T = 0$  and  $\mu_B = 0$ , where the phase transition is second order. At sufficient high temperature and  $\mu_I > \mu_c$ , the pion condensate evaporates and the spontaneous breaking  $I_3$  symmetry and parity are restored. The lattice calculations also suggest that the pion condensate vanishes for sufficient high  $\mu_I$  and this  $I_3$  symmetry restoration phase transition may be first order for large enough  $\mu_I$ . Therefore, there should exist a tricritical point (TCP) in the  $(T, \mu_I)$  phase diagram. We will show below that these conclusions can be verified in our calculations within the PNJL model.

Fig. 1 shows the temperature dependence of the pion condensate, chiral condensate and the trace of Polyakov loop at different  $\mu_I$ . In comparison with the zero  $\mu_I$  case, the magnitude

of chiral condensate is suppressed by the isospin chemical and it almost keeps as a constant until the pion condensate evaporates at high  $T'_c$ . The dependence of Polyakov loop  $\Phi$  on  $T$  is similar to the zero  $\mu_I$  case. In the low  $\mu_I$  region, the  $I_3$  symmetry restoration phase transition is second order. With increasing  $\mu_I$ , the evaporation of the pion condensate gets more and more abrupt and the  $I_3$  symmetry restoration phase transition eventually becomes first order. Fig. 1(c) shows that  $\Phi$  is also discontinuous at the first order phase transition point  $T'_c$ . This indicates there exists a TCP in the  $(T, \mu_I)$  phase diagram, which was first proposed in [36] by using lattice simulation. Fig.1 also shows that the  $I_3$  symmetry restoration phase transition temperature  $T'_c$  is always less than  $T_c^0$ .

Although chiral condensate is suppressed by the pion condensate, it still keeps considerable value in the low  $\mu_I$  region with  $\mu_I > \mu_c$ . Fig. 2 shows that the crossover phase transitions for the chiral condensate  $\sigma$  and for the Polyakov loop  $\Phi$  also perfectly coincide at  $T_c$  with  $T'_c < T_c < T_c^0$ . Therefore, if we define the peak of the Polyakov loop susceptibility<sup>1</sup> as the deconfinement phase transition point, the pion superfluidity phase is always confined at low  $\mu_I$  region. For high  $\mu_I$ , chiral condensate is greatly reduced and it has no meaning to compare the chiral susceptibility with the Polyakov loop susceptibility. Numerical results indicate that the peak of Polyakov loop susceptibility excellently coincides with the pion condensate vanishing point for high enough  $\mu_I$ , while for the not too large  $\mu_I$  the difference of these two points is within a few MeV. This points will be illustrated more clearly in the next section by considering a small  $I_3$  symmetry breaking term. Therefore, we get conclusion that the pion superfluidity phase is always confined.

The isospin chemical dependence of  $\sigma$ ,  $\pi$  and  $\Phi$  are plotted in Fig. 3. For a fixed  $T$ , the Polyakov loop  $\Phi$  is always a monotonic increasing function of  $\mu_I$  and the scaled chiral condensate is always a monotonic decreasing function of  $\mu_I$ . These points also qualitatively coincide with the lattice results [36, 37]. For  $T = 180\text{MeV}$ , pion superfluidity phase occurs at  $\mu_I = 75\text{MeV}$  which is very close to  $\mu_c$  and the phase transition is second order. The scaled pion condensate first increases with the increasing  $\mu_I$  and then decreases with the increasing  $\mu_I$  until it abruptly vanishes at  $\mu_I = 456\text{MeV}$ . With increasing  $T$ , the first order phase transition for the pion condensate vanishing becomes more and more soft and it evolves as a second order phase transition when  $T > 210\text{MeV}$ . Fig. 3 also shows that the two phase transition points for  $I_3$  symmetry breaking and restoration get more and more close to each other with the increasing  $T$  and eventually coincide at  $\sim(223\text{MeV}, 135\text{MeV})$ . Numerical results also suggest that the peak of  $\partial\Phi/\partial\mu_I$  is located at the vicinity of the pion condensate vanishing point.

The reason that the pion condensate first increases and then decreases with the increasing  $\mu_I$  at fixed  $T$  is that it eventually becomes energetically favourable to produce fermionic excitations

---

<sup>1</sup>In this paper the Polyakov loop susceptibility is defined as the partial differential of  $\Phi$  with respect to  $T$  or  $\mu_I$ . The definitions of the susceptibilities for chiral condensate and pion condensate are alike.

which then competes with the production of fermions in bound states with anti-fermions, that is pions. It is reasonable that to produce quark excitations gets more and more advantaged in contrast to the production of quarks in pions with anti-quarks for high  $T$ , as suggested by Fig.3. Since this phenomena is also observed at  $T \sim 223\text{MeV}$  where the non vanishing pion condensate (with very small value) only appears in the vicinity of  $\mu_I \sim 135\text{MeV}$ , we believe that the above result is not an effect due to the ultraviolet cutoff.

The  $(T, \mu_I)$  phase diagram of two flavor PNJL model is shown in Fig. 4(a), in comparison with the standard NJL phase diagram described by Fig. 4(b). We only plots the phase diagrams in the range  $\mu_I < 500\text{MeV}$  since the investigation for more high isospin chemical potential is beyond the capability of the NJL type models. The PNJL phase diagram is qualitatively consistent with the lattice results given in [37]. Fig. 4(a) shows that the pion condensate always vanishes above  $T_c^0$ . The TCP is located at  $(210\text{MeV}, 300\text{MeV})$ , which means that the phase transition for  $I_3$  symmetry restoration in the region  $\mu_I > 300\text{MeV}$  is always first order. In the rough, for  $\mu_I > 135\text{MeV}$ , the chiral condensate is greatly suppressed and the melting of pion condensate is simultaneously accompanied by the crossover phase transition for deconfinement; while for  $\mu_c < \mu_I < 135\text{MeV}$ , the chiral condensate still keeps a considerable value when the pion condensate vanishes and the crossover phase transitions for chiral symmetry restoration and deconfinement are still coincide. Note that numerical study suggests that the standard NJL model also sustain the existence of the TCP in the  $(T, \mu_I)$  phase diagram. The TCP obtained in standard NJL is at the vicinity of  $(140\text{MeV}, 400\text{MeV})$ . However, the standard NJL has no capability to give the information concerning the deconfinement phase transition.

### 3.2 The case for $\lambda \neq 0$ and $\mu_B = 0$

The previous lattice simulations for pion superfluidity phase transition are performed by introducing an explicit isospin symmetry term which is proportional to a small parameter  $\lambda$  in the lagrangian. The phase diagram is then obtained by extrapolating the results from  $\lambda \neq 0$  to  $\lambda = 0$ . To compare with the lattice data, we also investigate the  $\lambda \neq 0$  within PNJL formalism. In addition, studying  $\lambda \neq 0$  case can further deepen our understanding the role of the Polyakov loop dynamics .

with  $\lambda \neq 0$ , the pion condensate is no longer the true order parameter and the phase transition for pion superfluidity becomes a crossover. We perform the calculations with  $\lambda = 5\text{MeV}$  (with the same order as  $m_0$ ),  $0.5\text{MeV}$  and  $0.05\text{MeV}$ , respectively. Fig. 5 gives the scaled pion condensate, chiral condensate and Polyakov loop as functions of isospin chemical potential at  $\mu_B = 0$  and  $T = 210\text{MeV}$  for different  $\lambda$ . Fig. 5(a) shows that when  $\lambda = m_0$  the chiral condensate and pion condensate will have the same magnitude in vacuum, which indicates that a small explicit symmetry term has significant influence on the vacuum structure. With  $\lambda$

decreasing, the magnitude of  $\pi$  in  $\mu_I < \mu_c$  is greatly suppressed while its influence on the large  $\mu_I$  region is not so significantly. We can see that Fig. 5(c) which is obtained with  $\lambda = 0.05\text{MeV}$  is almost identical with Fig. 3(b) which is obtained with  $\lambda = 0$ . Fig. 5 also shows varying of small  $\lambda$  has little impact on the shape of Polyakov loop  $\Phi$ . Here we can get conclusion that the method taken in lattice simulation by extrapolating the results from  $\lambda \neq 0$  to  $\lambda = 0$  is reliable.

For small  $\lambda$ , we can use the peak of the pion condensate susceptibility to indicate the crossover phase transition for  $I_3$  symmetry breaking or restoration. In Fig. 6, we present  $\partial\pi/\partial\mu_I$  and  $\partial\Phi/\partial\mu_I$  obtained with the same parameters as Fig. 5. The curve of  $\partial\pi/\partial\mu_I$  has two peaks, which correspond to the crossover phase transitions for  $I_3$  symmetry breaking (the left peak) and  $I_3$  symmetry restoration (the right peak), respectively. It is shown that the peak of  $\partial\Phi/\partial\mu_I$  perfectly coincides with the right peak of  $\partial\pi/\partial\mu_I$ . Fig. 6 also shows that the peak position of  $\partial\Phi/\partial\mu_I$  is insensitive to the value of  $\lambda$  when  $\lambda \ll m_0$  while the extent of superposition between the peaks of  $\partial\Phi/\partial\mu_I$  and  $\partial\pi/\partial\mu_I$  is closely related to the magnitude of the explicit symmetry breaking term. In comparison with the Fig. 3(b), we find that the peak position of crossover phase transition for  $I_3$  symmetry breaking or restoration is considerably consistent with the corresponding true phase transition point for  $I_3$  symmetry breaking or restoration obtained with  $\lambda = 0$ . This results confirm that the melting of pion condensate for  $\mu_I > \mu'_c \approx 135\text{MeV}$  is simultaneously accompanied by the crossover deconfinement phase transition, just as shown in Fig. 4(a).

The evidence for the existence of TCP is illustrated in Fig. 7. Fixing  $\lambda = 0.5\text{MeV} \ll m_0$ , for high enough temperature ( $T > 210\text{MeV}$ ), the crossover phase transition for  $I_3$  symmetry breaking is similar to the crossover phase transition for  $I_3$  symmetry restoration, which indicates that both phase transitions are second orders for  $\lambda = 0$ ; While for the low enough temperature ( $T < 210\text{MeV}$ ), the right peak becomes significantly steeper than the left one, which indicates that it corresponds to a first order phase transition for  $\lambda = 0$ . Fig. 7 also shows that the two peaks get more and more close to each other with increasing  $T$  and eventually coincide at a point  $(T', \mu')$ . For  $\lambda \ll m_0$ , we find that the point  $(T', \mu')$  is almost identical with the point  $(223\text{MeV}, 135\text{MeV})$ .

Above results can also be confirmed by exploring the peak positions of  $\partial\pi/\partial T$  and  $\partial\Phi/\partial T$ , which is shown in Fig. 8. For low  $\mu_I = 80\text{MeV}$ , we can see that differences among three crossover phase transitions for chiral condensate, pion condensate and Polyakov loop are still within a few MeV with  $\lambda \approx m_0$ . For the same  $\lambda$ , the peaks related to the pion condensate and Polyakov loop both get more and more steep with increasing  $\mu_I$ , which implies that second order phase transition for  $I_3$  symmetry restoration eventually involves into the first order phase transition.

### 3.3 Comparison with Lattice results

For quantitative comparison with the corresponding lattice data, following [28], we also reduce the  $T_c^0$  by rescaling the parameter  $T_0$  from 270MeV to 190MeV. In this case, though the perfect coincidence of the crossovers for the deconfinement and chiral phase transitions is lost, the difference between the two transition is within 20MeV[28]. The average of these two temperatures can be defined as  $T_c^0$  with the value 180MeV, which is in the range of recent lattice results[46, 47]. Note that in the following calculations, we keep the liquid quark mass varying with the change of  $\beta$  and other parameters of the PNJL unchanged.

The PNJL results are compared with the lattice data obtained at fixed  $m = 0.05$ ,  $\mu_I = 0.4$  and  $\lambda = 0.005$  with  $N_t = 4$ [36] in Fig.9(the PNJL results were calculated with the same parameters). The critical  $\beta_c$  at zero chemical potential is 5.3198(9) for  $m=0.05$  [37], which may corresponds to  $T_c^0 = 180\text{MeV}$ . In lattice simulations with fixed  $N_t$ , the temperature  $T$  varies with lattice spacing  $a$  and  $T = N_t a^{-1}$ . Using 2-loop running of the coupling  $g(a)$ , the lattice spacing  $a$  can be expressed as

$$a = \Lambda_L^{-1} \left( \frac{6\beta_0}{\beta} \right)^{-\frac{\beta_1}{2\beta_0^2}} \exp\left(-\frac{\beta}{12\beta_0}\right), \quad (22)$$

where  $\beta = 6/g^2$ ,  $\beta_0 = \frac{1}{16\pi^2} \left( \frac{11N_c}{3} - \frac{2N_f}{3} \right)$  and  $\beta_1 = \frac{1}{(16\pi^2)^2} \left( \frac{34N_c^2}{3} - \frac{10N_c N_f}{3} - \frac{(N_c^2 - 1)N_f}{N_c} \right)$ . The one dimensional constant parameter  $\Lambda_L$  can be determined by comparing the known critical  $\beta_c$  with the corresponding critical temperature  $T_c^0$ . Using this relation, we can transform  $T$ s into  $\beta$ s and compare the PNJL results with the corresponding lattice data. Note that in lattice simulations, every quantity is made dimensionless by multiplying the appropriate power of  $a(\beta)$ .

Fig.9(a) shows that the dependence of Polyakov Loop on  $\beta$  in PNJL is well consistent with the lattice data. The peak of Polyakov Loop susceptibility from PNJL is located at  $\beta = 5.27$ , which coincides with the lattice result depicted in Fig.14 in Ref.[36]. With 2-loop running of the coupling  $g$ , this crossover transition point for deconfinement corresponds to  $T = 169\text{MeV}$  and  $\mu_I = 270\text{MeV}$  (note that  $\mu_I$  also changes with  $\beta$ ) with  $m = 34\text{MeV}$ . The variation of the pion condensate with respect to  $\beta$  is shown in Fig.9(b). Since the original data for pion condensate in [36] are all dimensionless quantities scaled by a series of physical units (corresponding to different lattice spacing  $a(\beta)$ ), we presented these data in physical units and then rescaled the obtained results by the pion condensate at  $\beta = 5.2$ . Both PNJL and lattice data show that the pion condensate first increases with  $\beta$  and then decreases with increasing  $\beta$ . The crossover phase transition for  $I_3$  symmetry restoration in PNJL model takes place at  $\beta = 5.3$  or ( $T = 175\text{MeV}$ ,  $\mu_I = 280\text{MeV}$ ) with  $m = 35\text{MeV}$ . In contrast with the critical value shown in Fig.9(a), both the temperature and isospin chemical potential of this point are shifted by less than 10MeV. We also performed calculations in PNJL for  $m = 0.05$  by keeping  $T_0 = 270\text{MeV}$  and adopting

$T_c^0 = 222\text{MeV}$  as in previous sections and found that both crossover transition points located at the same point  $\beta = 5.3$ . Therefore the coincidence of the crossover transitions for deconfinement and  $I_3$  symmetry restoration obtained in lattice simulation [36] can be successfully interpreted by including the Polyakov Loop dynamics in the NJL model.

The  $16^3 \times 4$  lattice simulations in [37] with the set of same parameters as in Fig.9 strongly suggest that there would be a first order phase transition for the  $I_3$  symmetry restoration between  $\beta = 0.525$  and  $\beta = 5.3$  in the  $\lambda \rightarrow 0$  limit. The authors of [37] claimed that this point is very close to the TCP. This first order phase transition was confirmed in our calculations within PNJL for  $\lambda = 0$  and the transition point is located at  $\beta = 5.32$  or ( $T = 180\text{MeV}$ ,  $\mu_I = 288\text{MeV}$ ), which is also in the vicinity of the TCP obtained in PNJL ( $m = 36\text{MeV}$ ).

At fixed  $\beta = 5.0$  or  $T = 119\text{MeV}$ , the pion condensate as a function of  $\mu_I$  for  $m = 0.05$  or  $m = 24\text{MeV}$  and different  $\lambda$  is plotted in Fig.10. The range of  $\mu_I$  in this plot corresponds to  $0 < \mu_I < 239\text{MeV}$ . The ellipses are the linear extrapolation of the lattice data to  $\lambda = 0$  and the solid line corresponds to the PNJL result obtained at  $\lambda = 0.0005$ . Fig.10 indicates that the PNJL results are quite well consistent with lattice data for  $\lambda = 0.01, 0.005$ . This plot also shows that the linear extrapolation to  $\lambda = 0$  in lattice simulation is in fairly good agreement with the PNJL data in the low and high  $\mu_I$  region, while the deviations are explicit in the vicinity of the true phase transition point. In contrast to the critical point  $\mu_I = 0.25(119\text{MeV})$  obtained from the lattice linear extrapolation, the critical isospin chemical potential in PNJL model is  $\mu_I = 0.3(143\text{MeV})$ . Both results sustain that the  $I_3$  symmetry broken phase transition is second order for low temperature (in contrast to  $T_c^0$ ) and no decrease of pion condensate with increase of  $\mu_I$  is observed in the plotted range of  $\mu_I$ .

## 4 Conclusion and outlook

The PNJL model represents a minimal synthesis of the two basic principles which govern QCD at low temperatures: spontaneous chiral symmetry breaking and confinement. In this work, we extended the two flavor Polyakov-loop-extended NJL model to the finite isospin chemical potential case, which can be investigated by lattice simulations. By including the pion condensate degrees of freedom, the trace of Polyakov loop and its conjugate can still be extracted out and the formalism which can simultaneously couple the fields of the pion condensate, chiral condensate and Polyakov loop is obtained.

Within this framework, the dependence of the pion condensate, chiral condensate and Polyakov loop on temperature and isospin chemical potential are explored and the two flavor  $(T, \mu_I)$  phase diagram is plotted at the mean field level. Our calculations confirmed that there exists a tri-critical point in the  $(T, \mu_I)$  phase diagram. In the low  $\mu_I$  region with pion condensate, the crossover phase transitions for chiral symmetry and deconfinement are still perfectly coincide

and the isospin symmetry restoration phase transition for high isospin chemical potential region is simultaneously accompanied with the crossover phase transition for deconfinement. We also directly compared the PNJL results with the corresponding lattice data at finite temperatures. In general, a qualitative agreement between these two methods is confirmed and in some cases even a quantitative agreement is obtained. Therefore, our results provides further test on the validity of this enhanced quasi-particle model. At the same time, the conclusions obtained within PNJL model also give a way to test the reliability of the lattice data for finite isospin density.

In this paper, we only explored the  $(T, \mu_I)$  phase structure of two flavor PNJL at zero baryon chemical potential. In our forthcoming paper, we will investigate the Polyakov loop dynamics on the phase structure, thermodynamic and meson properties at finite temperature, isospin chemical potential and baryon chemical potential. Further exploration on the phase diagram and meson properties of three flavor PNJL model by including the strangeness chemical potential is also underway.

## Acknowledgements

We are highly grateful to Dr. D.K. Sinclair for his helpful discussions on the detailed technique of lattice QCD simulations. This work was supported by National Natural Science Foundation of China under contract 10425521, 10575004 and 10675007, the key Grant Project of Chinese Ministry of Education (CMOE) under contract No.305001 and the Research Fund for the Doctoral Program of Higher Education of China under Grant No.20040001010. One of the author (LYX) thanks also the support of the Foundation for University Key Teacher by the CMOE.

## References

- [1] A. Casher, Phys. Lett. B **83**, 73 (1979).
- [2] A. Manohar and H. Georgi, Nucl. Phys. B **234**, 189 (1984).
- [3] T. Schaefer and E. Shuryak, Rev. Mod. Phys. **70**, 323-426 (1998)
- [4] J. Kogut *et al.*, Phys. Rev. Lett **50**, 393 (1983).
- [5] M. Fukugita and A. Ukawa, Phys. Rev. Lett. **57**, 503 (1986).
- [6] F. Karsch and E. Laermann Phys. Rev. D **50**, 6954 (1994).
- [7] S. Aoki *et al.*, Phys. Rev. D **57**, 3910 (1998).
- [8] F. Karsch, E. Laermann and A. Peikert, Nucl. Phys. B **605**, 579 (2001).

- [9] C. Gatttringer *et al.*, Phys. Rev. D **66**, 054502 (2002).
- [10] Z. Fodor, S. D. Katz, and K. K. Szabo, Phys. Lett. B **568**, 73 (2003).
- [11] Z. Fodor and S. D. Katz, JHEP **0203**, 014 (2002).
- [12] C. R. Allton *et al.*, Phys. Rev. D **66**, 074507 (2002).
- [13] C. R. Allton *et al.*, Phys. Rev. D **68**, 014507 (2003).
- [14] C. R. Allton *et al.*, Phys. Rev. D **71**, 054508 (2005).
- [15] E. Laermann and O. Philipsen, Ann. Rev. Nucl. Part. Sci. **53**, 163 (2003).
- [16] P. de Forcrand and O. Philipsen, Nucl. Phys. B **673**, 170 (2003)
- [17] M. D’Elia and M. P. Lombardo, Phys. Rev. D **67**, 014505 (2003).
- [18] M. D’Elia and M. P. Lombardo, Phys. Rev. D **70**, 074509 (2004).
- [19] Y. Nambu and G. Jona-Lisinio, Phys. Rev. **122**, 345 (1961); Phys. Rev. **124**, 246 (1961).
- [20] K.P. Klevansky, Rev. Mod. Phys. **64**, 649 (1992).
- [21] T. Hatsuda and T. Kunihiro, Phys. Rept. **247**, 221 (1994).
- [22] M. Buballa, Phys. Rept. **407**, 205-376 (2005).
- [23] P. N. Meisinger and M. C. Ogilvie, Phys. Lett. B **379**, 163 (1996).
- [24] P. N. Meisinger, T. R. Miller, and M. C. Ogilvie, Phys. Rev. D **65**, 034009 (2002).
- [25] K. Fukushima, Phys. Lett. B **591**, 277 (2004).
- [26] A. Mocsy, F. Sannino and K. Tuominen, Phys. Rev. Lett. **92**, (2004) 182302
- [27] E. Megias, E. Ruiz Arriola and L. L. Salcedo, arXiv:hep-ph/0412308.
- [28] C. Ratti, M. A. Thaler and W. Weise, Phys. Rev. D **73**, 014019 (2006).
- [29] K. Fukushima, Ann. Phys. **304**, 72 (2003).
- [30] S. K. Ghosh, T. K. Mukherjee, M. G. Mustafa and R. Ray, Phys. Rev. D **73**, (2006) 114007
- [31] P. N. Meisinger, M. C. Ogilvie and T. R. Miller, Phys. Lett. B **585**, 149 (2004).
- [32] C. Ratti, S. Rößner, M. A. Thaler and W. Weise, arxiv: hep-ph/0609218.

- [33] S. Rößner, C. Ratti and W. Weise, arxiv: hep-ph/0609281.
- [34] D. T. Son and M. A. Stephanov. Phys. Rev. Lett. **86** , 592 (2001); Phys. At. Nucl. **64**, 834 (2001).
- [35] J.B. Kogut and D.K. Sinclair, Nucl. Phys. B **106** (Proc Suppl), 444 (2001).
- [36] J. B. Kogut and D. K. Sinclair, Phys. Rev. D **66**, 034505 (2002);
- [37] J. B. Kogut and D. K. Sinclair, Phys. Rev. D **70** , 094501 (2004).
- [38] S. Mukherjee, M. G. Mustafa and R. Ray, arxiv: hep-ph/0609249.
- [39] A.Barducci, R.Casalbuoni, G.Pettini, L.Ravagli, Phys.Lett. **B 564**, 217(2003)
- [40] D.Toublan and J.B.Kogut, Phys.Lett. **B564**, 212(2003)
- [41] A.Barducci, R.Casalbuoni, G.Pettini, L.Ravagli, Phys.Rev. **D 71**, 016011(2005)
- [42] L.He, M.Jin and P.Zhuang, Phys.Rev.**D71**, 116001(2005)
- [43] B.Klein, D.Toublan and J.J.M.Verbaarschot, Phys.Rev. **D 72**, 015007(2005)
- [44] Y.Nishida, Phys.Rev.**D 69**, 094501(2004)
- [45] Z.Zhang and Y.X.Liu, hep-ph/0603252, Phys. Rev. **C 75**, 035201(2007)
- [46] M. Cheng *et al.* (RBC-Bielefeld collaboration), Phys. Rev. D **74**, 054507 (2006)
- [47] Y. Aoki, Z. Fodor, S. D. Katz and K. K. Szabo, Phys. Lett. B **643**, 46 (2006)

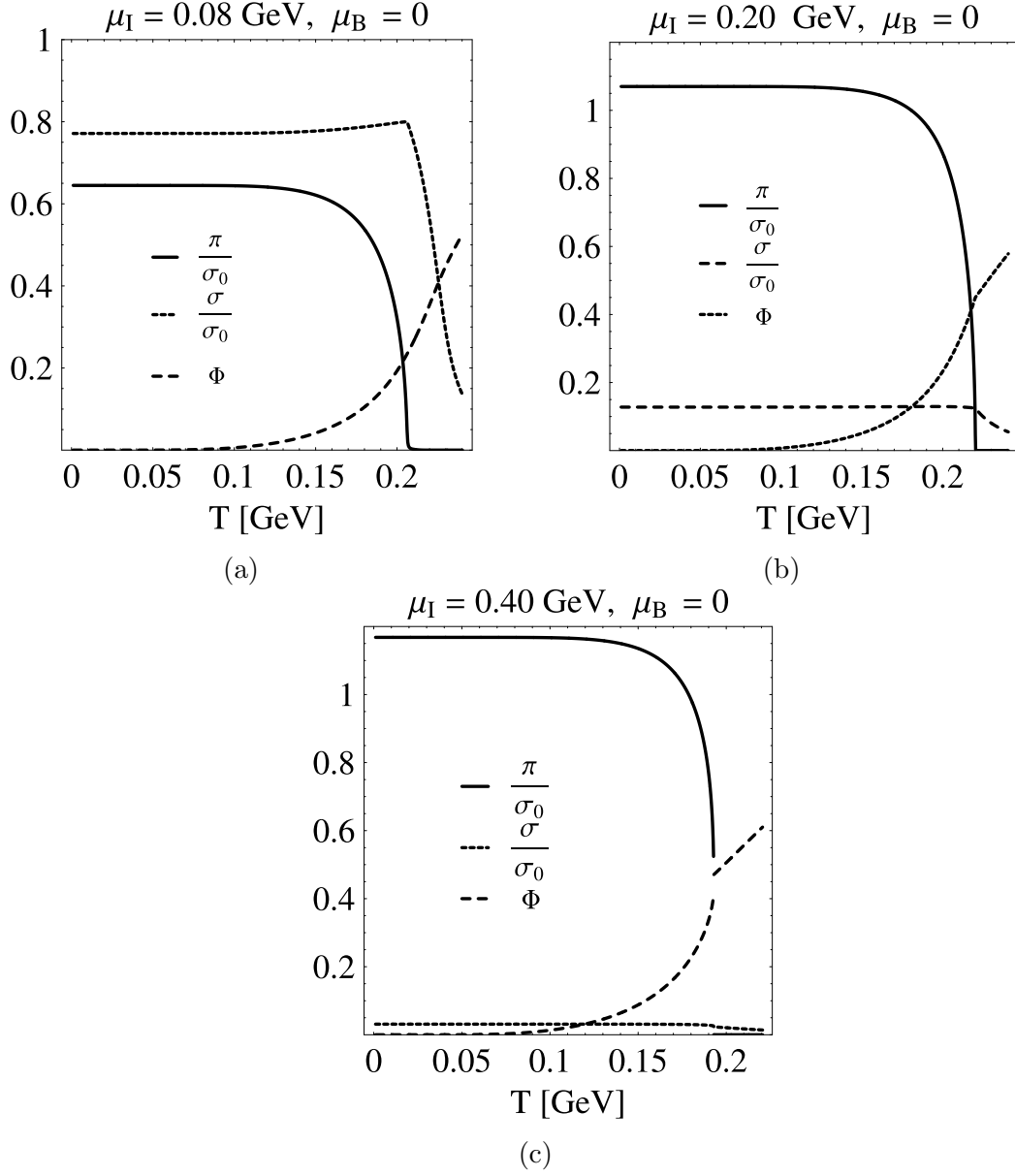


Figure 1: Scaled pion condensate, chiral condensate and Polyakov loop  $\Phi$  as functions of temperature at zero baryon chemical potential for different  $\mu_I$  with  $\lambda = 0$ .

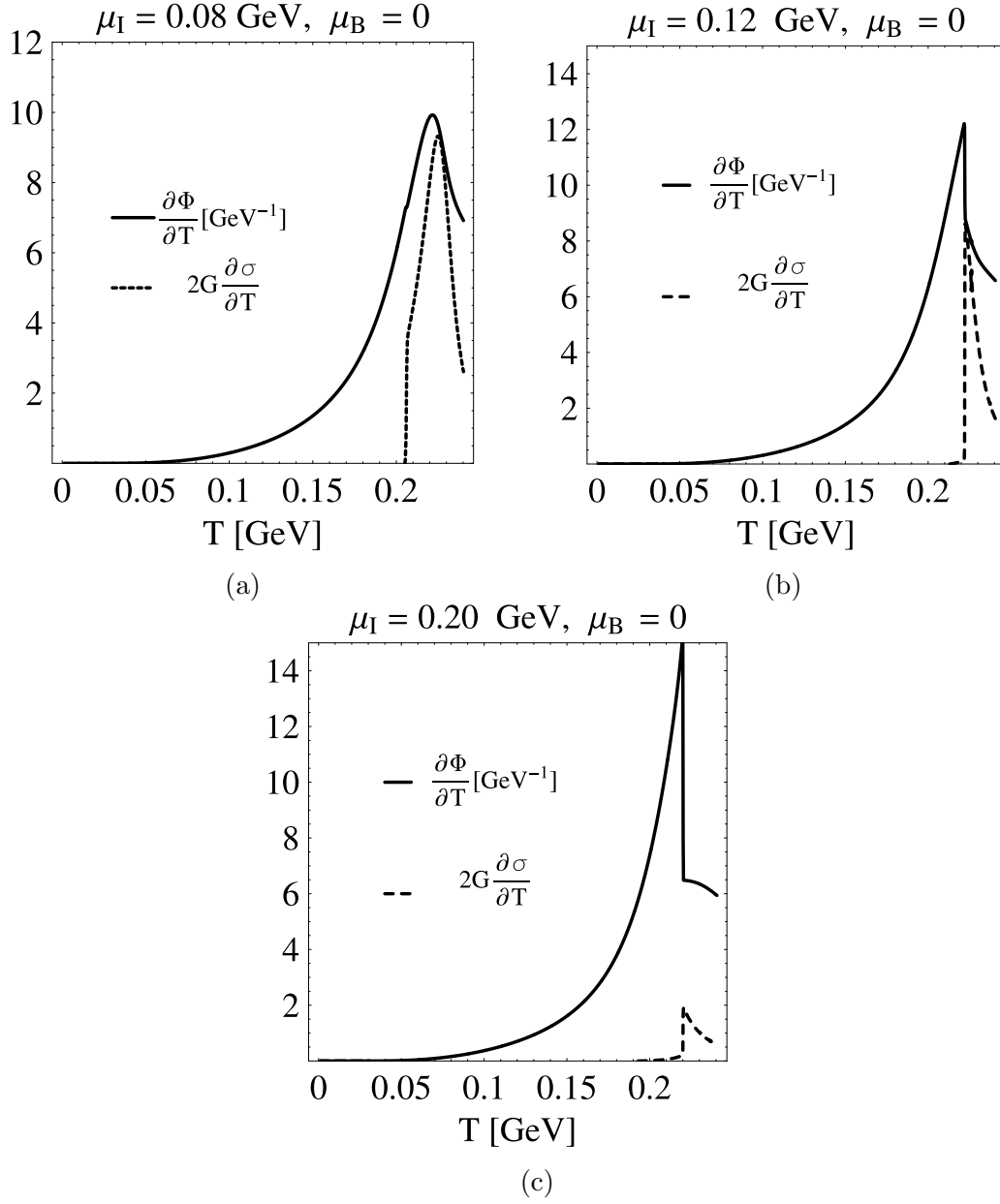


Figure 2: Plots of  $\partial(2G\sigma)/\partial T$  and  $\partial\Phi/\partial T$  for different  $\mu_I$  with  $\lambda = 0$ .

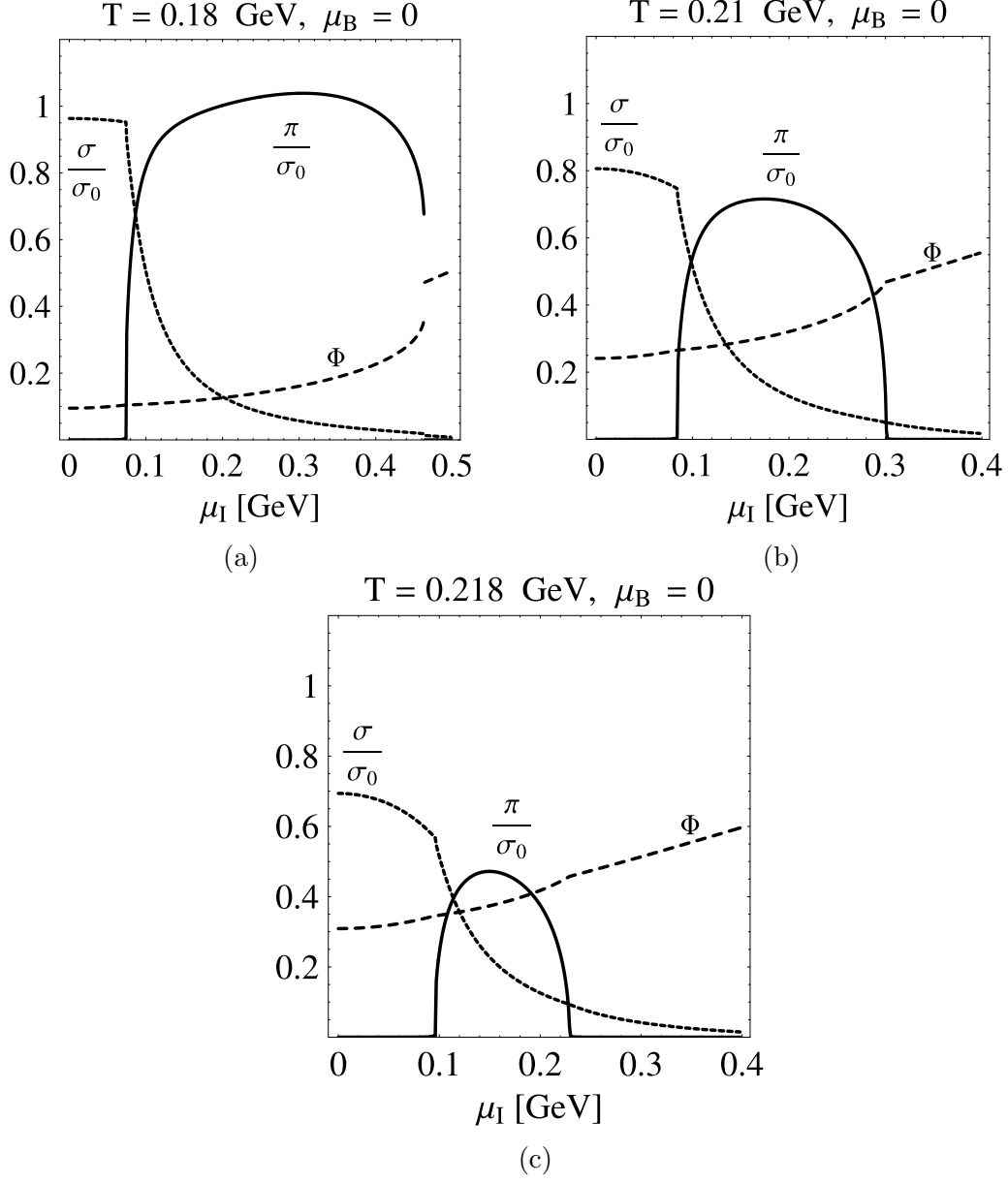


Figure 3: Scaled pion condensate, chiral condensate and Polyakov loop  $\Phi$  as functions of isospin chemical potential at zero baryon chemical potential for different  $T$  with  $\lambda = 0$ .

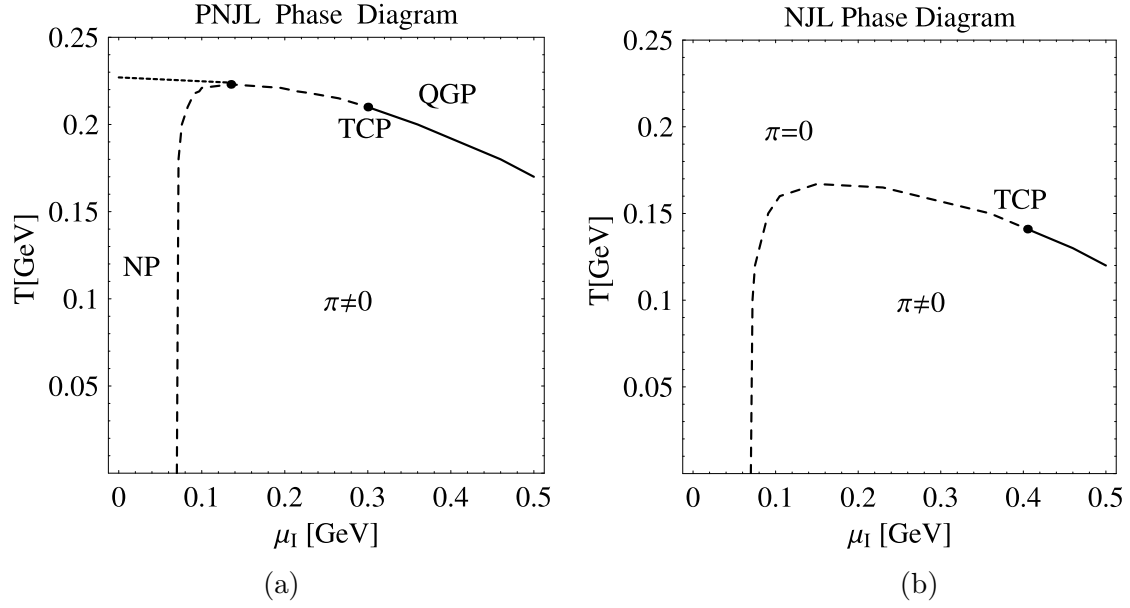


Figure 4: The  $(T, \mu_I)$  phase diagrams of two flavor PNJL (Left) and standard NJL (Right). NP stands for normal hadronic phase and QGP stands for quark-gluon plasma phase. The solid line (dashed line) stands for the first order ( second order ) pion superfluidity phase transition. The dotted line in the left panel indicates the crossover for deconfinement phase transition.

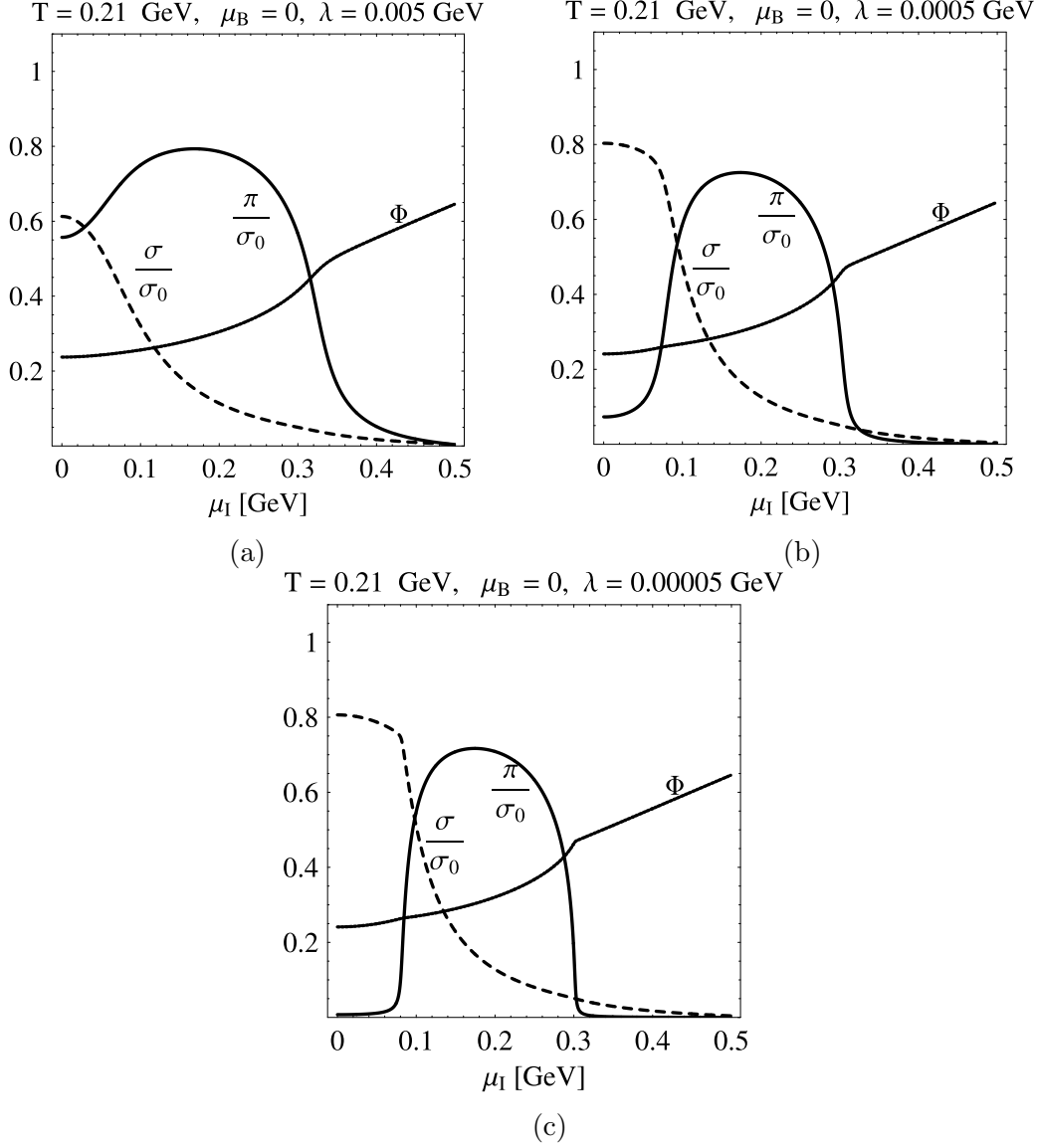


Figure 5: Scaled pion condensate, chiral condensate and Polyakov loop  $\Phi$  as functions of isospin chemical potential at zero baryon chemical potential for  $T = 210$  MeV with different  $\lambda \neq 0$ .

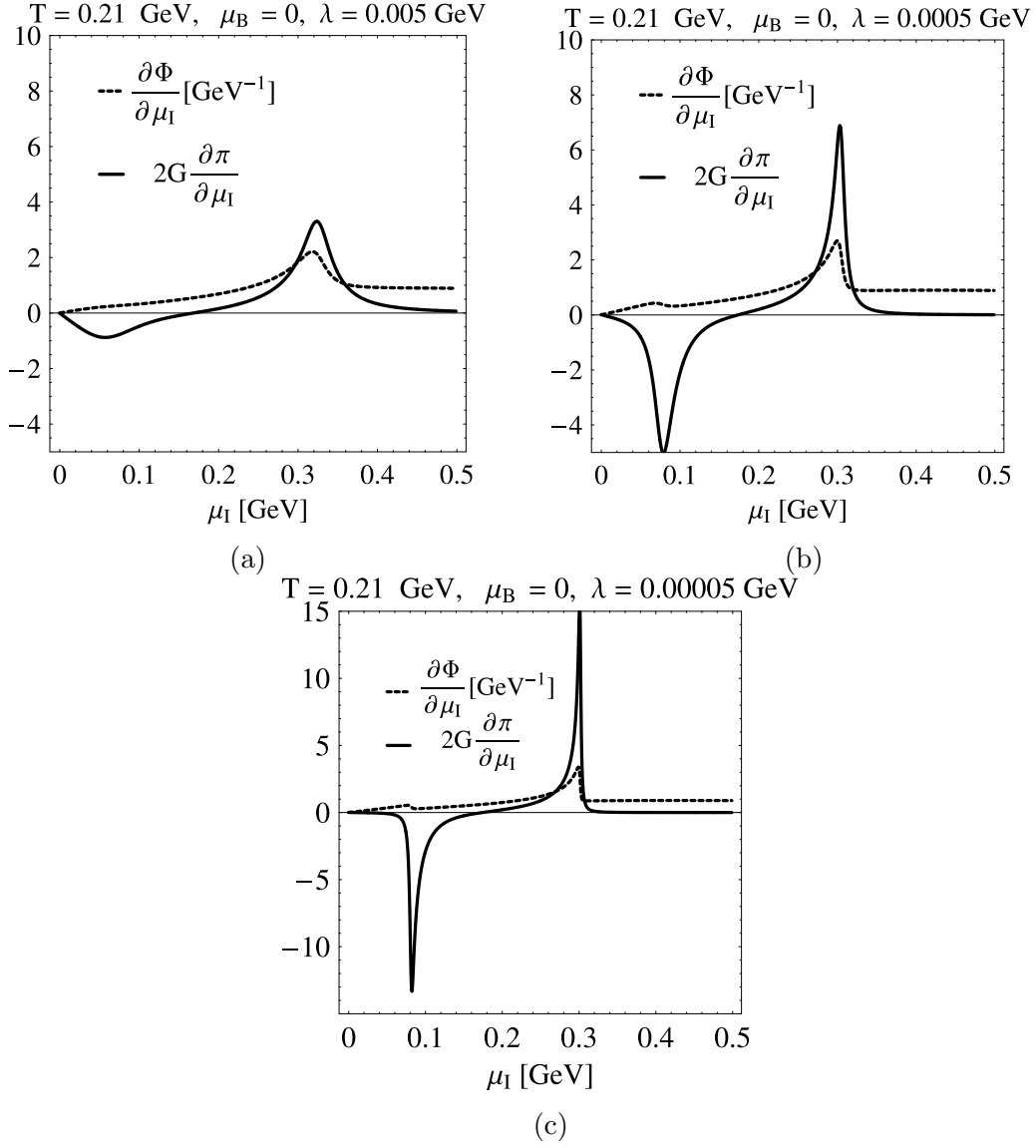
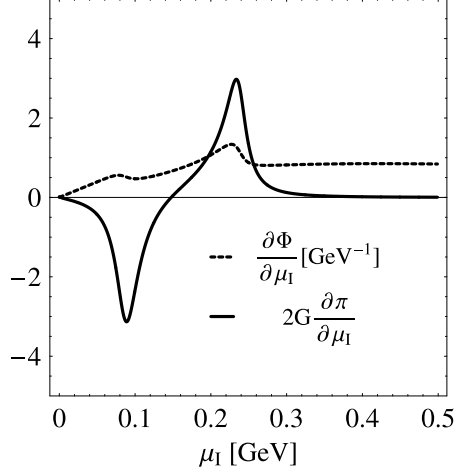


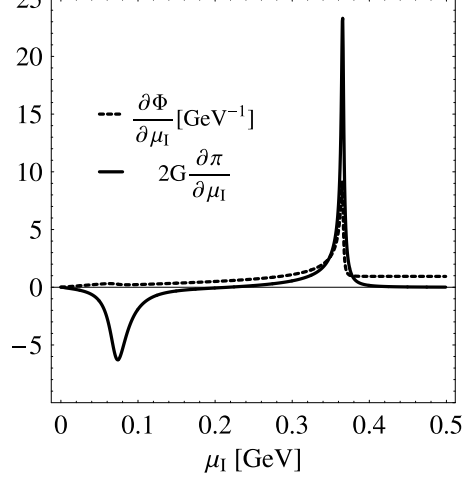
Figure 6: Plots of  $\partial(2G\pi)/\partial\mu_I$  and  $\partial\Phi/\partial\mu_I$  as functions of  $\mu_I$  for  $T = 210\text{MeV}$  and  $\mu_B = 0$  with different  $\lambda$ .

$T = 0.218 \text{ GeV}, \mu_B = 0, \lambda = 0.0005 \text{ GeV}$



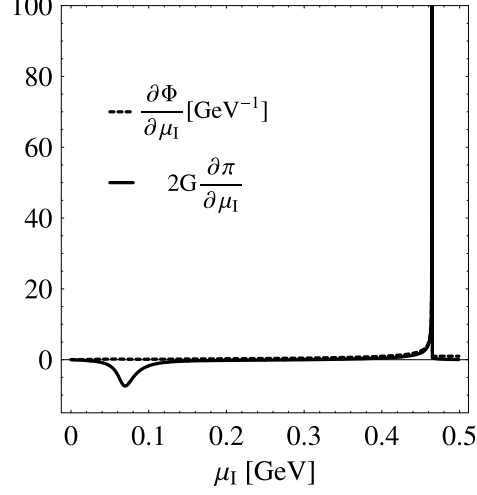
(a)

$T = 0.20 \text{ GeV}, \mu_B = 0, \lambda = 0.0005 \text{ GeV}$



(b)

$T = 0.18 \text{ GeV}, \mu_B = 0, \lambda = 0.0005 \text{ GeV}$



(c)

Figure 7: Plots of  $\partial(2G\pi)/\partial\mu_I$  and  $\partial\Phi/\partial\mu_I$  as functions of  $\mu_I$  at  $\lambda = 0.5\text{MeV}$  for different temperature.

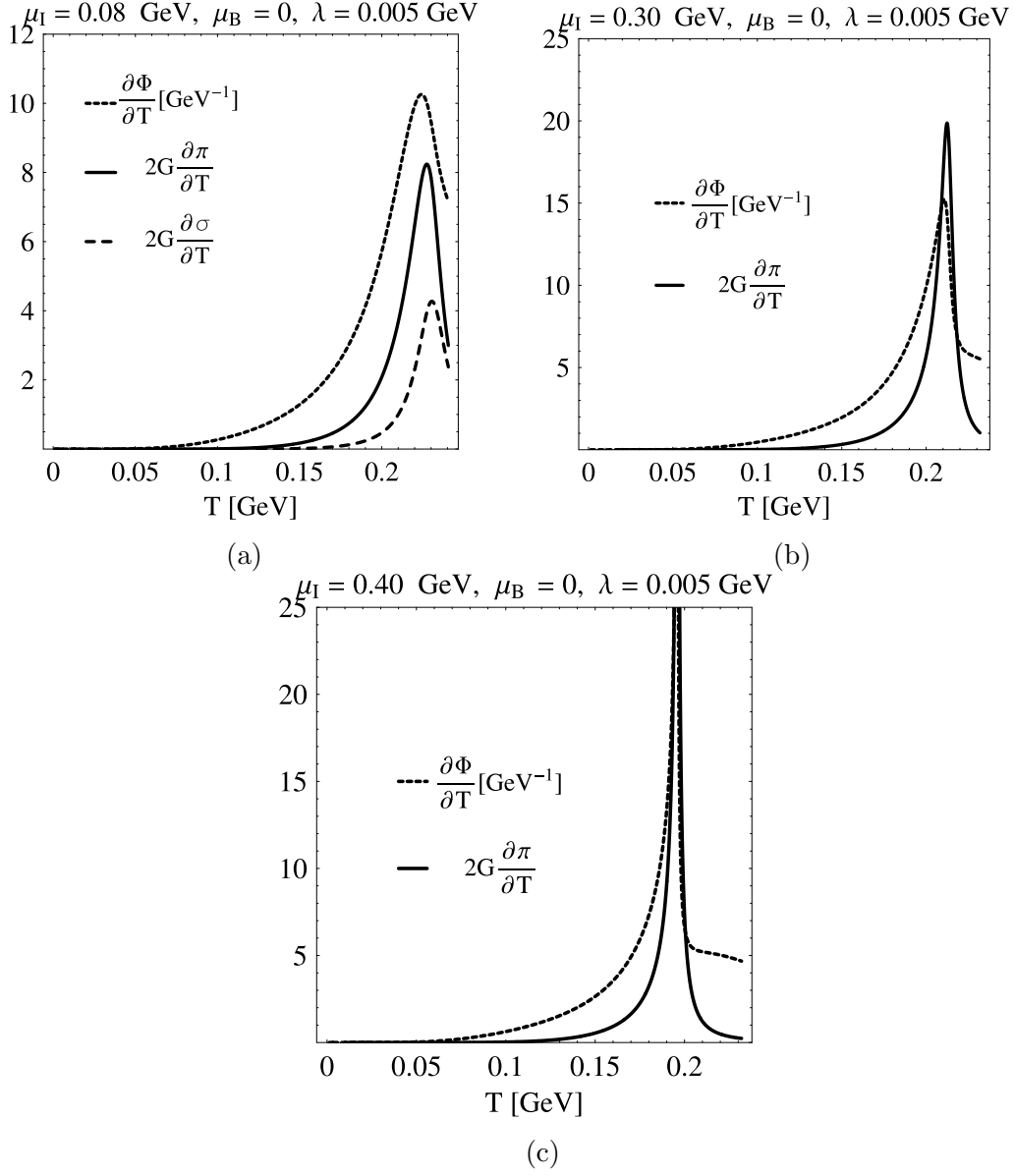


Figure 8: Plots of  $\partial(2G\sigma)/\partial T$ ,  $\partial(2G\pi)/\partial T$  and  $\partial\Phi/\partial T$  as functions of  $T$  for different  $\mu_I$  with the same  $\lambda$ .

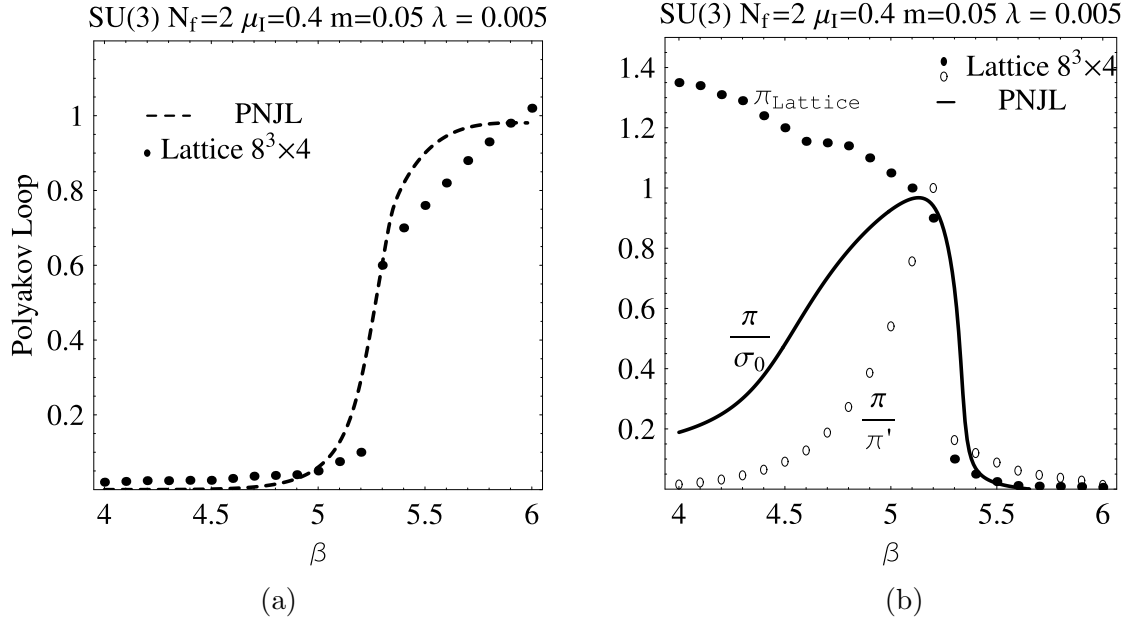


Figure 9: Polyakov Loop and pion condensate as a function of  $\beta$ . The lattice data (the black circles) are taken from [36] for  $m = 0.05$ ,  $\lambda = 0.005$  on an  $8^3 \times 4$  lattice. In the right panel, the white circles correspond to the original lattice data which were first represented in the same physical units and then rescaled by the obtained pion condensate at  $\beta = 5.2(\pi')$ .

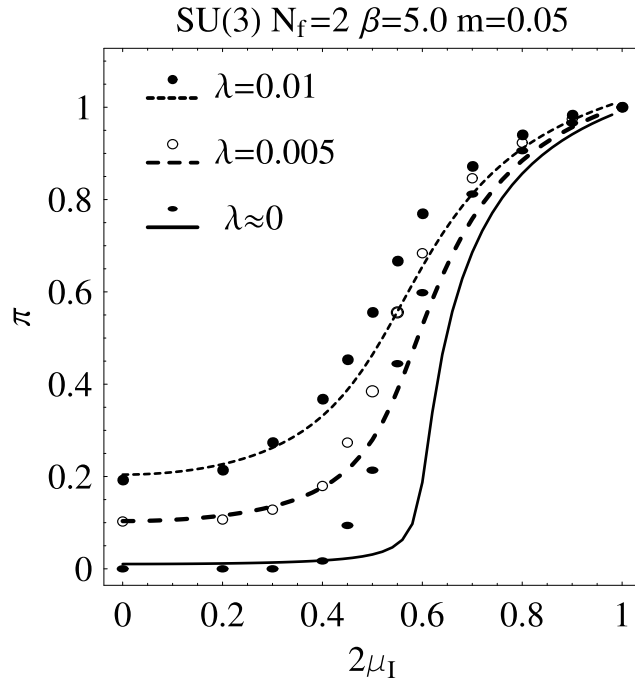


Figure 10: Scaled pion condensate as function of  $\mu_I$  for  $\lambda = 0.01$ ,  $\lambda = 0.005$  and  $\lambda \rightarrow 0$  at fixed  $m=0.05$  and  $\beta = 5.0$ . The lattice data are taken from [36] and we rescaled them by the lattice result for the pion condensate at  $2\mu_I = 1$  and  $\lambda = 0.01$ . The curves for the PNJL data are also scaled by the pion condensate obtained in PNJL at  $2\mu_I = 1$  and  $\lambda = 0.01$ .